3. Comparative diagnosis of Canine Elbow Dysplasia between Radiography, Computer Tomography and Arthroscopy

3.1 Materials and Methods

3.1.1 Dogs

Ninety-two elbow joints of sixty-one dogs which were arthroscopically explored during 2004 to 2006 at the Clinic for Small Domestic Animals, Free University of Berlin, because of elbow lameness were perspectively evaluated. The breed and sex of the 61 dogs are given in Table 1. To be included each dog had to have adequately documented clinical records, a complete radiographic and CT study of both elbow joints, and an arthroscopic study of clinically affected joints. The age range was four months to ten years with a mean of 33 months, and 36 dogs were more than 12 months old. Their bodyweights ranged from 16 to 65 kg with a mean of 31 kg, and when the condition was diagnosed they had been lame for between three weeks and two years. Thirty dogs were affected bilaterally. The final diagnosis was based on the identification by arthroscopy of a subchondral defect or a bony fragment associated with medial coronoid process of ulna.

Table 1: Breed and sex distribution of 61 dogs with FMCP

Breeds	Male	Female	Total
Bernese Mountain dog	1	2	3
Golden Retriever	7	3	10
Rottweiler	2	1	3
Labrador Retriever	13	4	17
German Shepherd	1	4	5
Mix	3	4	7
Beagle	1	0	1
Bulldog	1	2	3
Newfoundland	0	1	1
Munsterlander	2	0	2
Australian Shepherd	1	0	1
Rhodesian Ridgeback	1	0	1
Boxer	1	0	1
French Mastiff	1	0	1
Staffordshire bull terrier	0	1	1
Briard	1	0	1
German Wachtel	0	1	1
Airedale	0	1	1
Great Dane	1	0	1
Total	**37**	**24**	**61**

Table 2: Breed and affected joint distribution of 61 dogs (92 joints) with FMCP

Breeds	Unilateral	Bilateral	Total
Bernese Mountain dog	1	2	3
Golden Retriever	5	5	10
Rottweiler	2	1	3
Labrador Retriever	7	10	17
German Shepherd	1	4	5
Mix	4	3	7
Beagle	1	0	1
Bulldog	2	1	2
Newfoundland	0	1	1
Munsterlander	1	1	2
Australian Shepherd	1	0	1
Rhodesian Ridgeback	1	0	1
Boxer	1	0	1
French Mastiff	0	1	1
Staffordshire bull terrier	1	0	1
Briard	0	1	1
German Wachtel	1	0	1
Airedale	1	0	1
Great Dane	1	0	1
Total	**31**	**30**	**61**

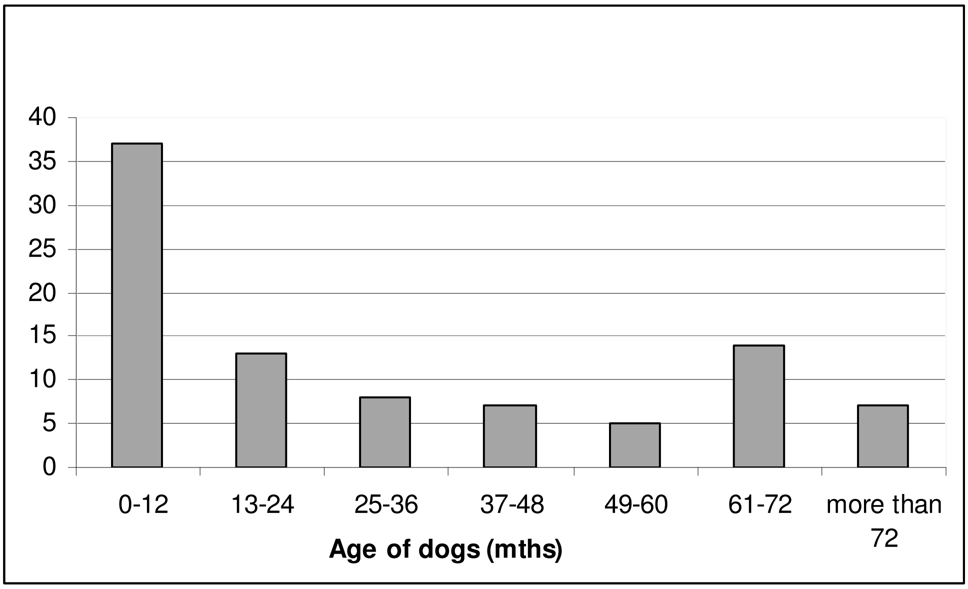

Fig. 8 Age distribution of 61 dogs with FMCP or FMCP/OCD undergoing Computer Tomography and Arthroscopy

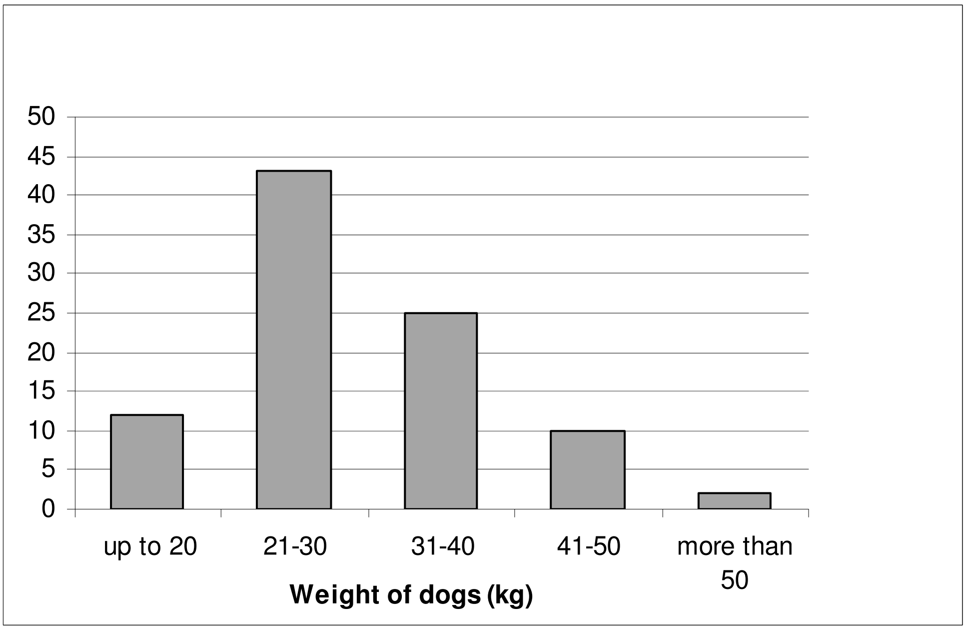

Fig. 9 Weight distribution of 61 dogs with FMCP or FMCP/OCD undergoing Computer Tomography and Arthroscopy

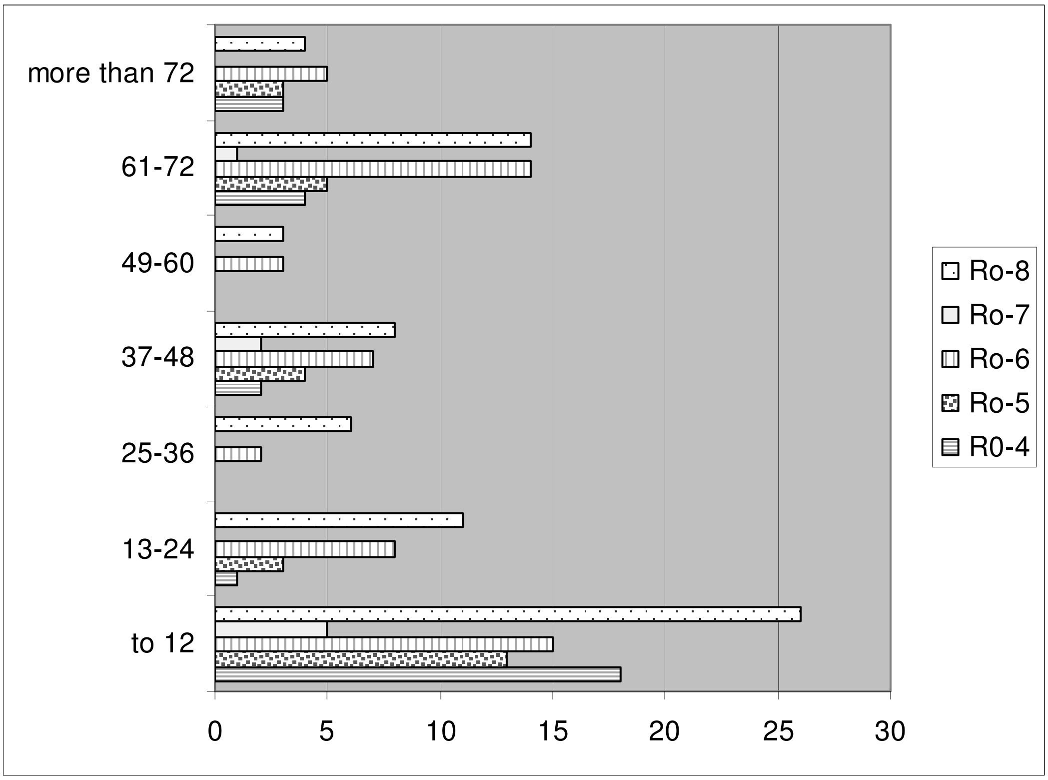

Fig. 10 Box plot of age distribution of dogs with FMCP or FMCP/OCD and Radiographic findings from lateral projection

Ro-4 = lateral projection seen osteophytes at proximal non articular surface of the anconeal process
Ro-5 = lateral projection seen osteophytes at dorso proximal radial head
Ro-6 = lateral projection seen osteophytes at proximal aspect of the medial coronoid process
Ro-7 = lateral projection seen osteophytes at lateral epicondyle of the humerus
Ro-8 = lateral projection seen osteophytes at subtrochlear region of the ulna

3.1.2 Radiographic examination

After the physical examination, both elbow joints were examined radiographically while each dog was sedated with a combination of Midazolam (0.05 mg/kg), and Propofol (6 mg/kg). Using a table-top technique, craniocaudal and flexed mediolateral projections were taken with a 300 mA, 150 kVp x-ray unit (Philips, OPTIMUS 50, kVp setting was between 50 and 55) with a focal film distance of 100 cm. Orthochromatic film was used in combination with rare earth intensifying screens.

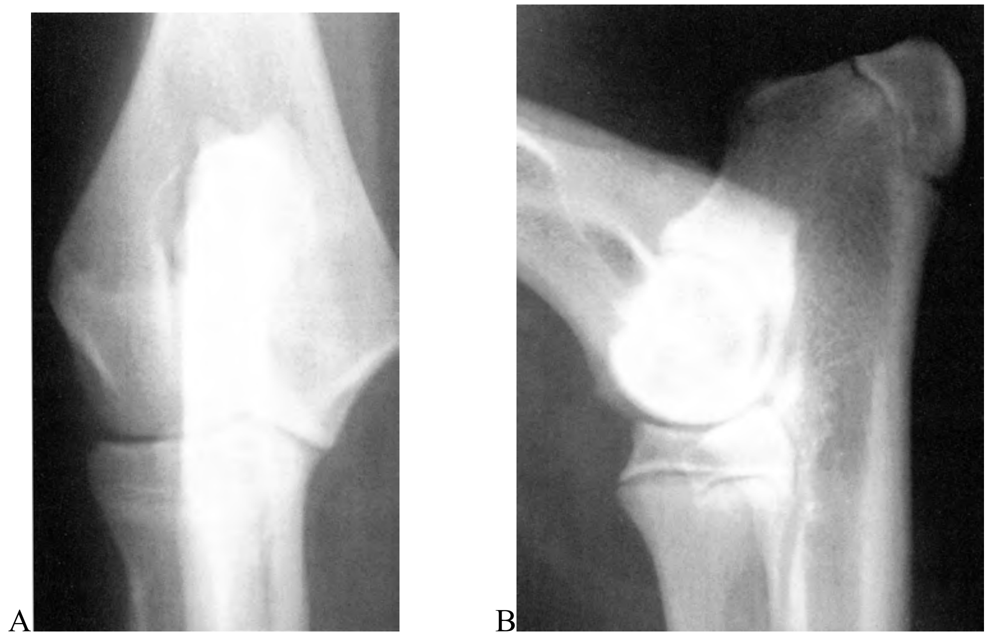

Fig. 11 Craniocaudal (A) and mediolateral (B) radiographs of a normal elbow joint

Each joint was evaluated for signs of soft tissue swelling, OCD lesion at the medial aspect of the humeral trochlea and periarticular formation at the medial coronoid process of the ulna (MCP) or the medial epicondyle of the humerus from craniocaudal projection (Fig. 6).

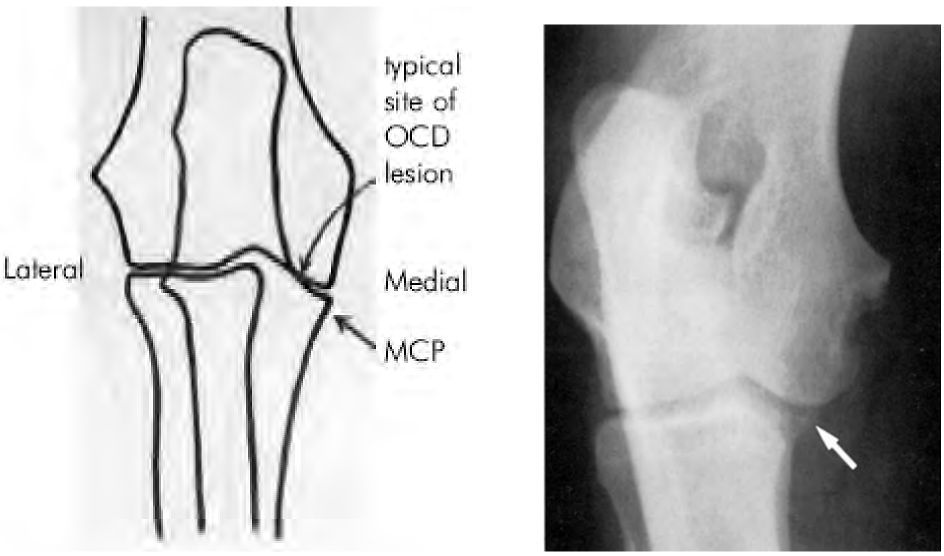

Fig. 12 The true craniocaudal is the best projection from which to diagnose Osteochondritis dissecans. The typical site of an OCD lesion is the medial aspect of the humeral trochlea (also referred to as the medial humeral condyle) (WORTH, 2001; MORGAN, 2000).

The flex mediolateral projections were evaluated and showed the presence of osteophytes in five locations. These projections are in accordance with the recommendations of the International Elbow Working Group (Fig. 13 to Fig. 17).

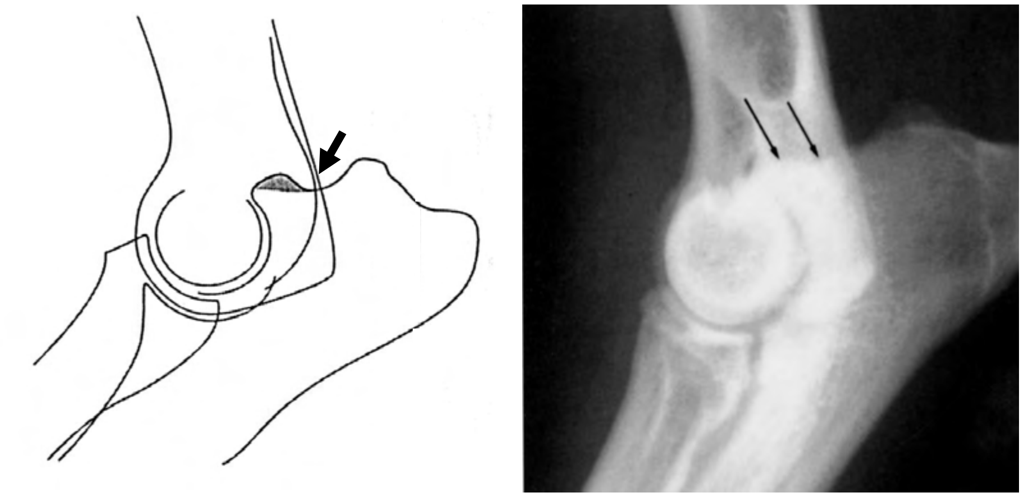

Fig. 13 The proximal non-articular surface of the anconeal process. The shaded area represents the site of early osteophytes production.

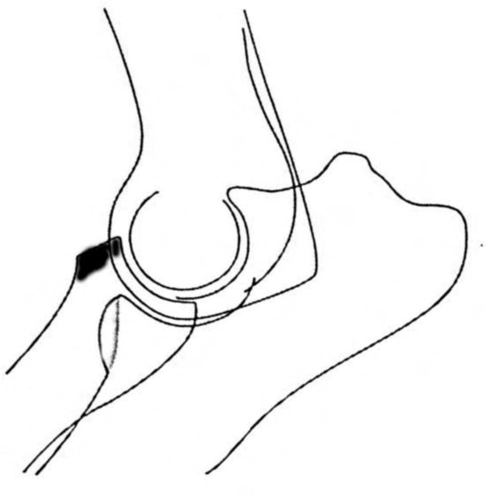

Fig. 14 The dorso-proximal radial head. The shaded area represents the area that should be evaluated for increased bone density.

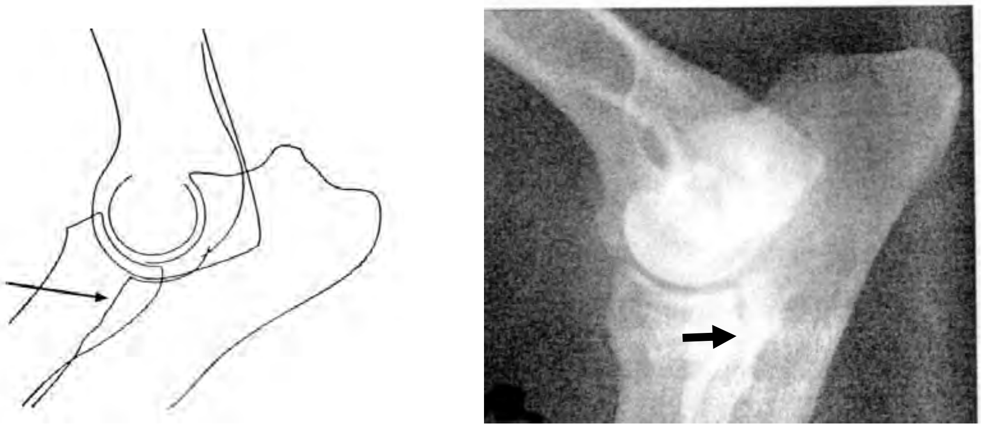

Fig. 15 Thin arrow represents the area of proliferative changes associated with the proximal aspect of the medial coronoid process. Thick arrow demonstrates altering the shape of the medial coronoid process because of proliferative changes.

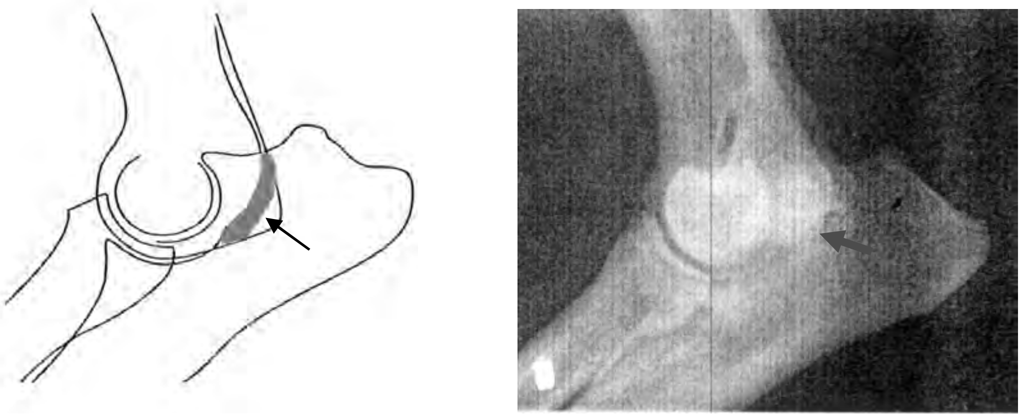

Fig. 16 The lateral epicondyle of the humerus. Shaded areas specify the area in which proliferation occurs, it can be detected as an contour shape of lateral epicondyle of the humerus (thick arrow).

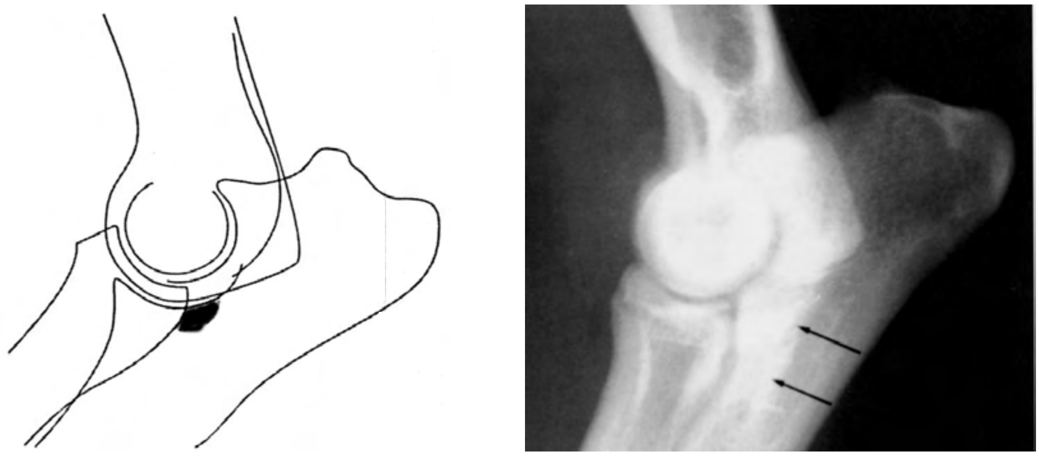

Fig. 17 The subtrochlear region of the ulna (seen as sclerosis). The shaded area represents the area that should be evaluated for increased bone density.

3.1.3 CT examination

After the radiographic examination, a CT examination was carried out under general anesthesia, induced with 0.3 mg/kg Propofol (Narcofol) via intravenous injection, and maintained with Isofluran (1 to 2 percent). CT scans of the elbow were obtained using the third-generation CT scanner (GE light speed). The dogs were placed in dorsal recumbency, the elbows were set in slightly cranial extension. Then the elbows were scanned in pairs. The region to be scanned was identified using an initial craniocaudal scout projection and included the entire elbow articulation distal to the coronoid process. This region of interest was scanned with sequential slices at 1.0 mm intervals, slice thickness was 1.25 mm. Reconstructions were made by using a bone setting (window width 2000 Hounsfield units, window level 350 Hounsfield units). The images were evaluated for the presence of fragmentation at the medial coronoid process of the ulna and determined whether separated fragment or in situ fragment. Each joint was evaluated for signs of degenerative joint disease (new bone formation at the distal end of the humerus, proximal radial head and medial coronoid process of the ulna. The difference CT images were reconstructed in multiple anatomical planes to evaluate incongruence between radius und ulna.

Fig. 18 The third-generation CT scanner (GE light speed) which was used in this experiment

Fig. 19 The dog position for CT examination. The dogs were placed in dorsal recumbency and elbows were in slight extension.

3.1.4 Arthroscopic examination

The clinically affected joints were examined by arthroscopy. During the arthroscopic examination, the status of synovial membrane, the articular cartilage, and the visibility of the fragment were evaluated. The articular cartilage was evaluated for signs of irregularity or erosion. The visibility of any fragments was evaluated for visualizing whether fragment or fissure line. If they were visible, the fragments were removed arthroscopically. The subchondral bone was curetted and the joint was lavaged with Ringer’s solution. The synovitis was classified as moderate and severe. In a joint with moderate synovitis, synovial villi were moderately enlarged, had a simple form and did not fill the joint completely, so that the joint structures were still visible. In a joint with severe synovitis, the synovial villi were greatly enlarged, had a more complex form and filled the joint space completely, covering most of the structures. Figures 20 to 27 show instruments for small animal arthroscopy.

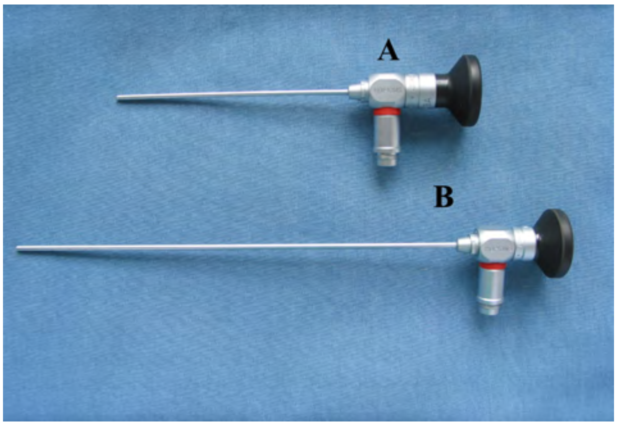

A: 1.9 mm short 30 degrees oblique

B: 2.7 mm long 30 degrees oblique

Fig. 20 Arthroscope for elbow joint

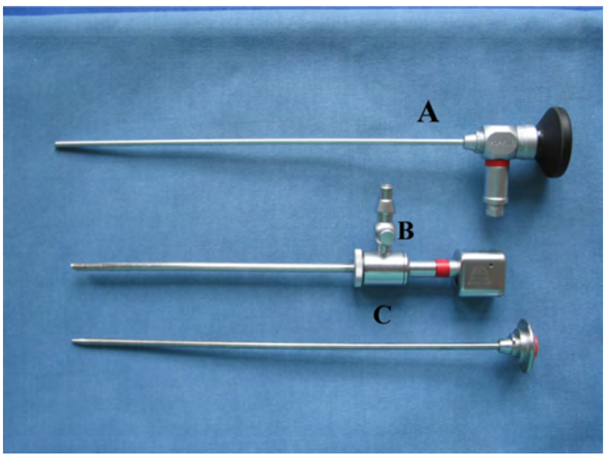

A: Arthroscope

B: Cannula

C: Trocar

Fig. 21 Small arthroscope cannula system

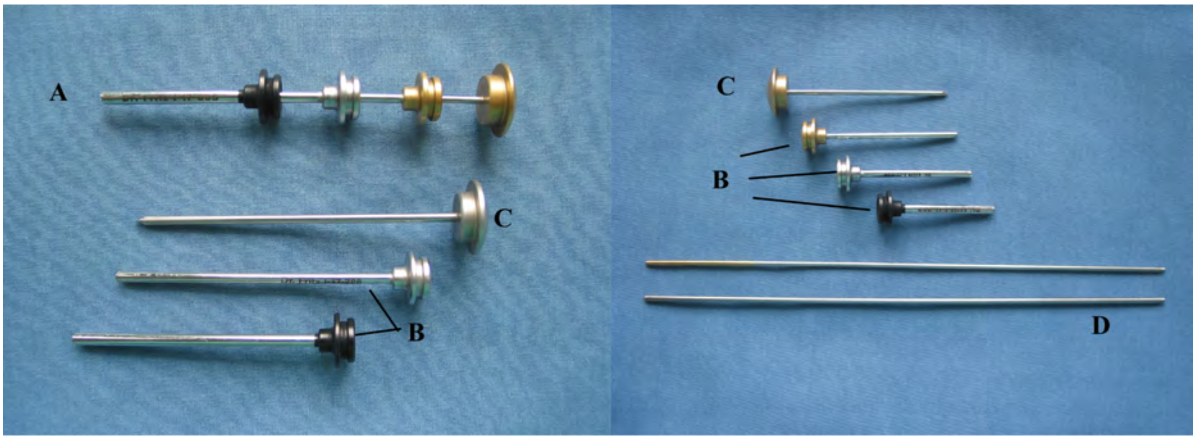

Fig. 22 Veterinary small-joint cannula system
A: Assembled system
B: Cannulas
C: Trocar
D: Switching sticks

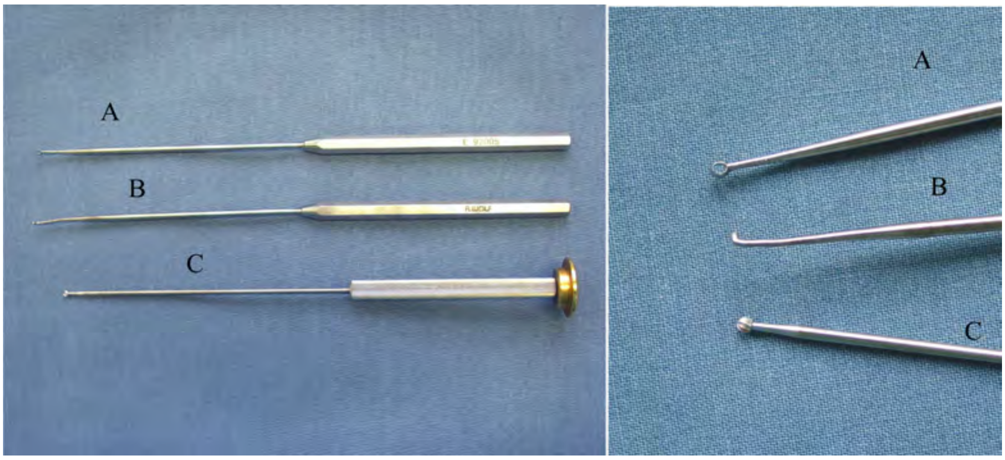

Fig. 23 Veterinary arthroscopic instruments
(A) Arthroscopic ring with close up
(B) Right-angle probes with close up projections of the tip
(C) Arthroscopic hand burr with a close up projection of the tip

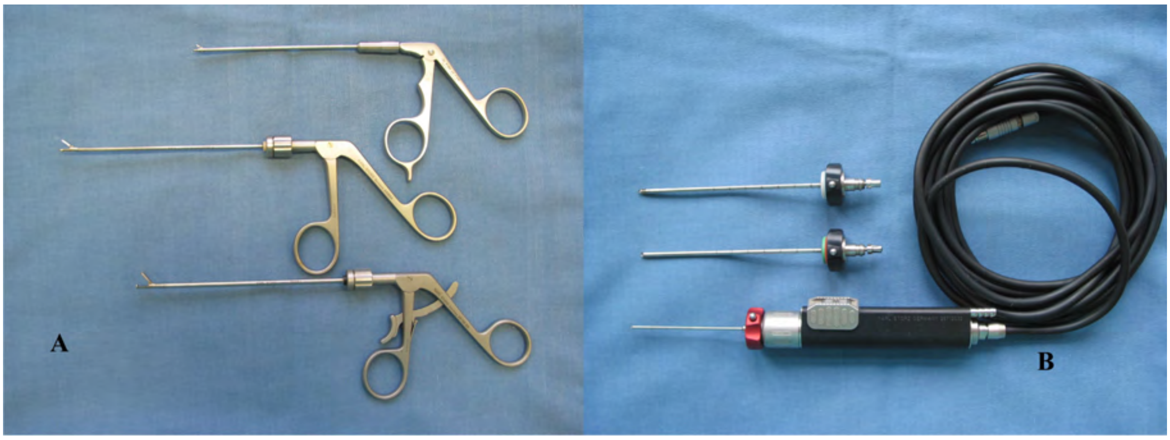

Fig. 24 (A) Arthroscopic grasping forceps (B) Small- joint hand piece for an arthroscopic shaver

Fig. 25 (A) Control box for veterinary video camera system (B) and camera head

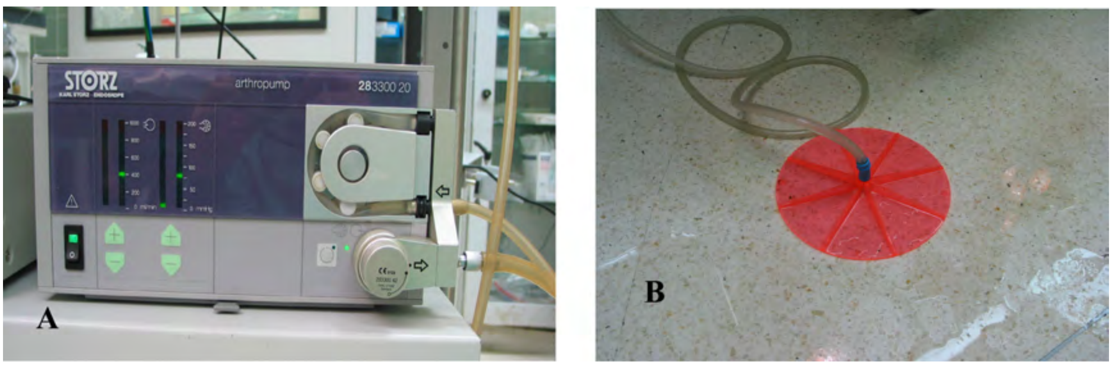

Fig. 26 (A) Control box for an arthroscopic pump and (B) Floor suction unit

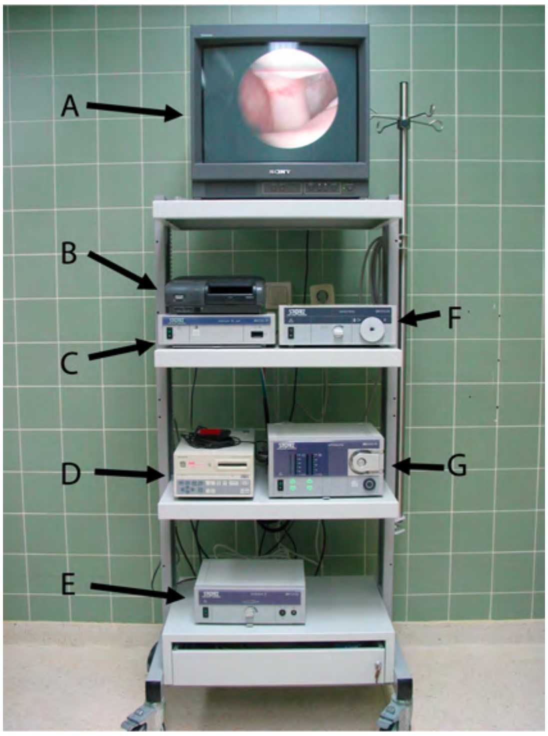

A: Monitor
B: Videocassette recorder
C: Control box for a camera
D: Device to capture still images
E: Control box for a shaver
F: Light source
G: Control box for pumping

Fig. 27 Arthroscopic tower

3.2 Evaluation of findings and statistical analysis

The radiographic and CT findings were compared with arthroscopy findings in terms of accuracy, sensitivity, specificity, positive and negative predictive values for each of the techniques. These terms were calculated by using the formulae Altmann (1997), which is demonstrated in Table 3.

Table 3: The formulae used to calculate the accuracy, sensitivity, specificity, positive and negative predictive values for each of the techniques (Altmann, 1997)

Parameter	Formula
Accuracy	Number of correct diagnoses by radiography or CT present/ total number of diagnosis
Sensitivity	Number of true positives by radiography or CT present/ total number of true positives by arthroscopy
Specificity	Number of true negatives by radiography or CT present/ total number of true negatives by arthroscopy
Positive predictive value	Number of true positives by radiography or CT present/ total number of positives by radiography or CT
Negative predictive value	Number of true negatives by radiography or CT present/ total number of negatives diagnoses by radiography or CT

3.3 Results

3.3.1 Radiographic findings

Radiographic lesions were found in 78 of the 92 (84%) elbow joints examined (61 dogs). There were bilateral FMCP lesions in 25 of the 61 dogs. On the craniocaudal projection there was evidence of OCD at the medial aspect of the humeral trochlea in 3 joints (3.2%). Fragmented medial coronoid process was seen in 20 of the 92 joints (21.7%). There was radiographic evidence of degenerative joint disease or periarticular new bone formation in 24 joints (26%). The most radiographic findings on flexed mediolateral projection are sclerosis at the subtrochlear region of the ulna. We have seen osteophyte at this location in 60 of the 92 joints (65.2%). The second area where we can mostly detect new bone formation is the proximal aspect of the medial coronoid process. The abnormal radiographic findings present at this area were in 41 joints of the 92 joints (44.5%). There were 20 joints (21.7%), 19 joints (20.6%) and 3 joints (3.2%) in which were observed osteophytes at the dorso-proximal radial head, the proximal non-articular surface of the anconeal process and the lateral epicondyle of the humerus respectively.

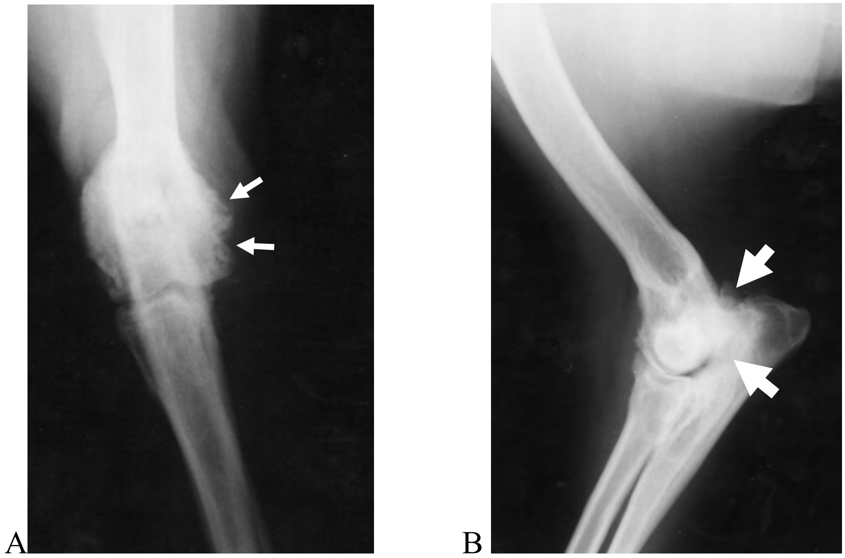

Fig. 28 Craniocaudal (A) and Flexed mediolateral (B) radiographic projections of a 2-years-old Labrador dog with severe arthrosis and FMCP. Radiographic signs include sclerosis of the trochlear notch *(thick arrow)* and osteophyte formation on the medial epicondyle of the humerus and coronoid process *(arrows)*.

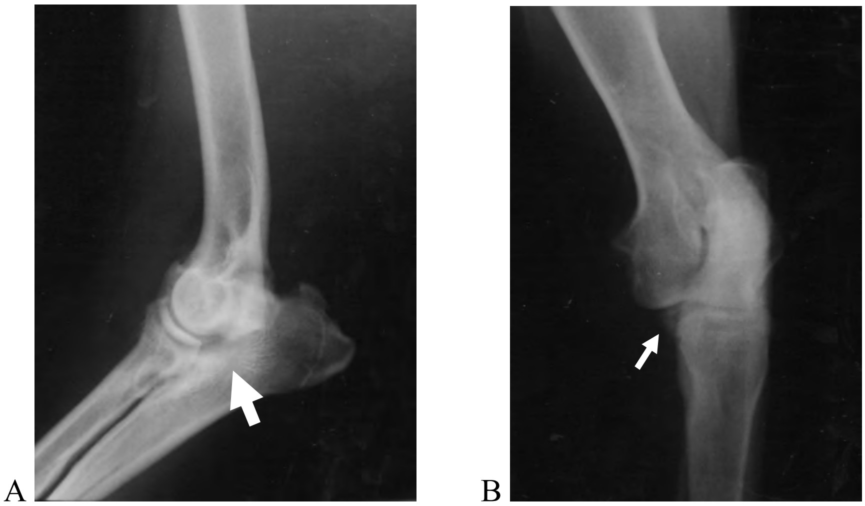

Fig. 29 Flexed mediolateral (A) and craniocaudal (B) radiographic projections of a 6-month-old Bernese Mountain dog with FMCP. Radiographic signs include sclerosis of the trochlear notch *(thick arrow)* and osteophytes formation on the medial epicondyle of the humerus and coronoid process *(arrows)*.

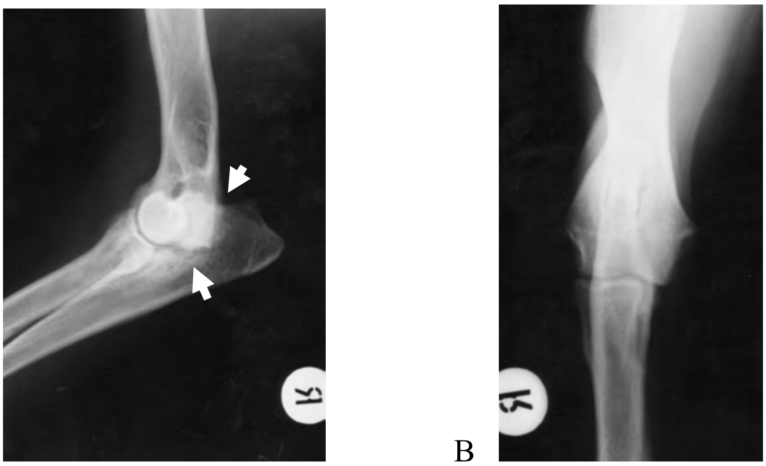

A B

Fig. 30 Flex mediolateral (A) and craniocaudal (B) radiographic projections of a 3-years-old German Shepherd dog with FMCP. Radiographic signs include sclerosis of the trochlear notch *and* osteophytes formation on the proximal edge of the anconeal process *(thick arrow)* on lateral projection. By craniocaudal projection no abnormal radiographic findings.

Table 4: Radiographic findings in 92 elbows (61 dogs) with FMCP

Radiographic findings		Number	Percentage
Craniocaudal projection	OCD lesion at trochlea of humerus	3	3.2 (3/92)
	Fragment visible at medial coronoid process	20	21.7 (20/92)
	Osteophytes at MCP or epicondyle of humerus	24	26 (24/92)
Flexed mediolateral projection	Osteophytes at the proximal non-articular surface of the anconeal process	19	20.6 (19/92)
	Osteophytes at the dorso-proximal radial head	20	21.7 (20/92)
	Osteophytes at the proximal aspect of the medial coronoid process	41	44.5 (41/92)
	Osteophytes at the lateral epicondyle of the humerus	3	3.2 (3/92)
	Sclerosis at the subtrochlear region of the ulna	60	65.2 (60/92)

3.3.2 CT findings

By CT examination were found 73 FMCP lesions in 92 elbow joints (79.3%). The most CT findings that were detected are periarticular bone formations 60 joints of 92 joints (65.2%). Separated fragments were present in 24 joints (26%) and in situ fragments in 38 joints (41.3%). Periarticular new bone formations were seen in 32 joints of 38 joints (84%) which had in situ fragments, and 22 joints of 24 joints (91%) which had separated fragments. We could diagnose joint incongruence in 8 joints of 92 joints (8.6%) and, 3 of them had also periarticular new bone formation.

Table 5: Computer Tomographic findings in 92 elbows (61 dogs) with FMCP

CT findings	Number	Percentages (%)
Separated fragments	24	26 (24/92)
Fissure line/ in situ fragments	38	41.3 (38/92)
Periarticular new bone formation	60	65.2 (60/92)
Joint incongruence	8	8.6 (8/92)

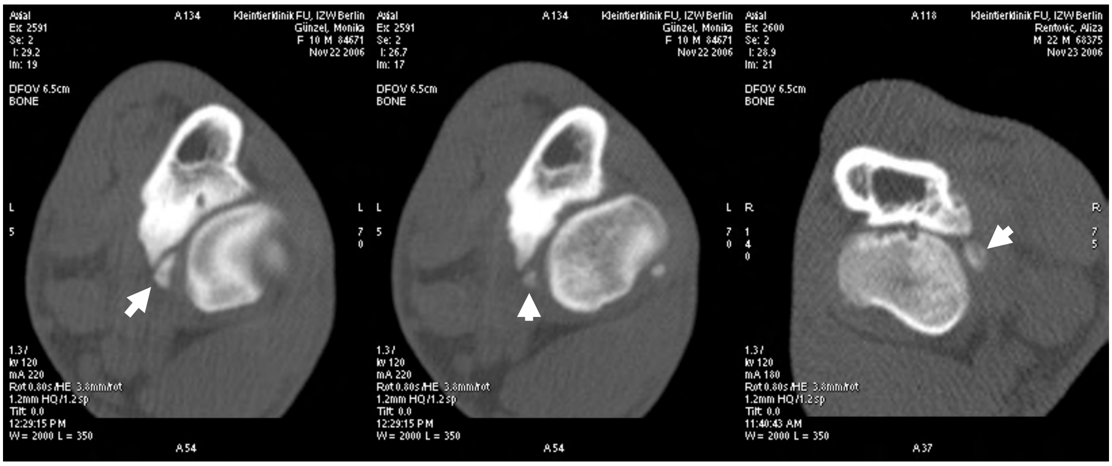

A **B** **C**

D **E** **F**

Fig. 31 CT images of a 5-year-old Labrador elbow with fragmented medial coronoid process of ulna
(A), (B) axial image from left elbow with separated fragment of MCP
(C) axial image from right elbow with in situ fragmented MCP
(D), (E) oblique image from left elbow with FMCP
(F) sagittal image from right elbow with FMCP

A B C

Fig. 32 Radiographic image, CT image and 3D-CT image of a 1-year-old French Mastiff elbow with fragmented medial coronoid process of ulna
(A) Radiographic signs include sclerosis of the trochlear notch *and* osteophyte formation on the proximal edge of the anconeal process.
(B) axial image from right elbow with separated fragment of MCP
(C) 3D-CT image with separated fragment of medial coronoid process

A B

Fig. 33 CT image and 3D-CT image of a 3-year-old Golden Retriever elbow with fragmented medial coronoid process of ulna
(A) axial image from right elbow with in situ fragment of MCP
(B, C) 3D-CT image with in situ fragment (arrows) of medial coronoid process

A.

B.

Fig. 34 CT image and 3D-CT image of a 1-years-old Golden Retriever elbow with severe arthrosis and displaced fragmented medial coronoid process of ulna
(A) axial image from right elbow with displaced fragment of MCP
(B) 3D-CT image with displaced fragment (arrows) of medial coronoid process and corpora libra (arrow head)

A.

B.

Fig. 35 CT image and 3D-CT image of a 2-year-old Golden Retriever elbow with severe arthrosis and non-displaced fragmented medial coronoid process of ulna
(A) axial image from right elbow with severe arthrosis
(B) 3D-CT image with joint arthrosis (arrow)

3.3.3 Arthroscopic findings

The abnormal findings were found in eighty-five joints of ninety-two joints (92.3%) which were examined by arthroscopy. Synovitis was evident in 56 joints (60.8%) of 85 affected joints. Only in 19 joints of 56 joints (20.6%) severe synovitis was found. By arthroscopy we could find fragments of subchondral bone at medial coronoid process in 59 elbows (64.1%), and in 56 elbows (60.8%) we could find cartilage erosion. Moreover, joint incongruence was present in 13 joints of 85 joints (14.1%). 38 elbows of 56 elbows (67.8%) that have cartilage erosion have synovitis. Twenty one of them had moderate synovitis and 17 of them (30%) had severe synovitis. Synovitis was observed in joints which have fragments of subchondral bone at MCP in 32 elbows that had synovitis. Most of them 81 %(26/32) had moderate synovitis. Three of thirteen (23%) joints presented incongruence with cartilage erosion and fragmented subchondral bone and 6 of 13 (46%) elbows have incongruence with cartilage erosion.

Table 6. Arthroscopic lesion of 92 elbows with FMCP

Arthroscopic findings		Number	Percentage (%)
Synovitis		56	60.8 (56/92)
	Moderate	37	40.2 (37/92)
	Severe	19	20.6 (19/92)
Cartilage erosion		56	60.8 (56/92)
Fragmented subchondral bone at MCP		59	64.1 (59/92)
	Non-displaced fragments	41	44.5 (41/92)
	Displaced fragments	18	19.5 (18/92)
Joint incongruence		13	14.1 (13/92)

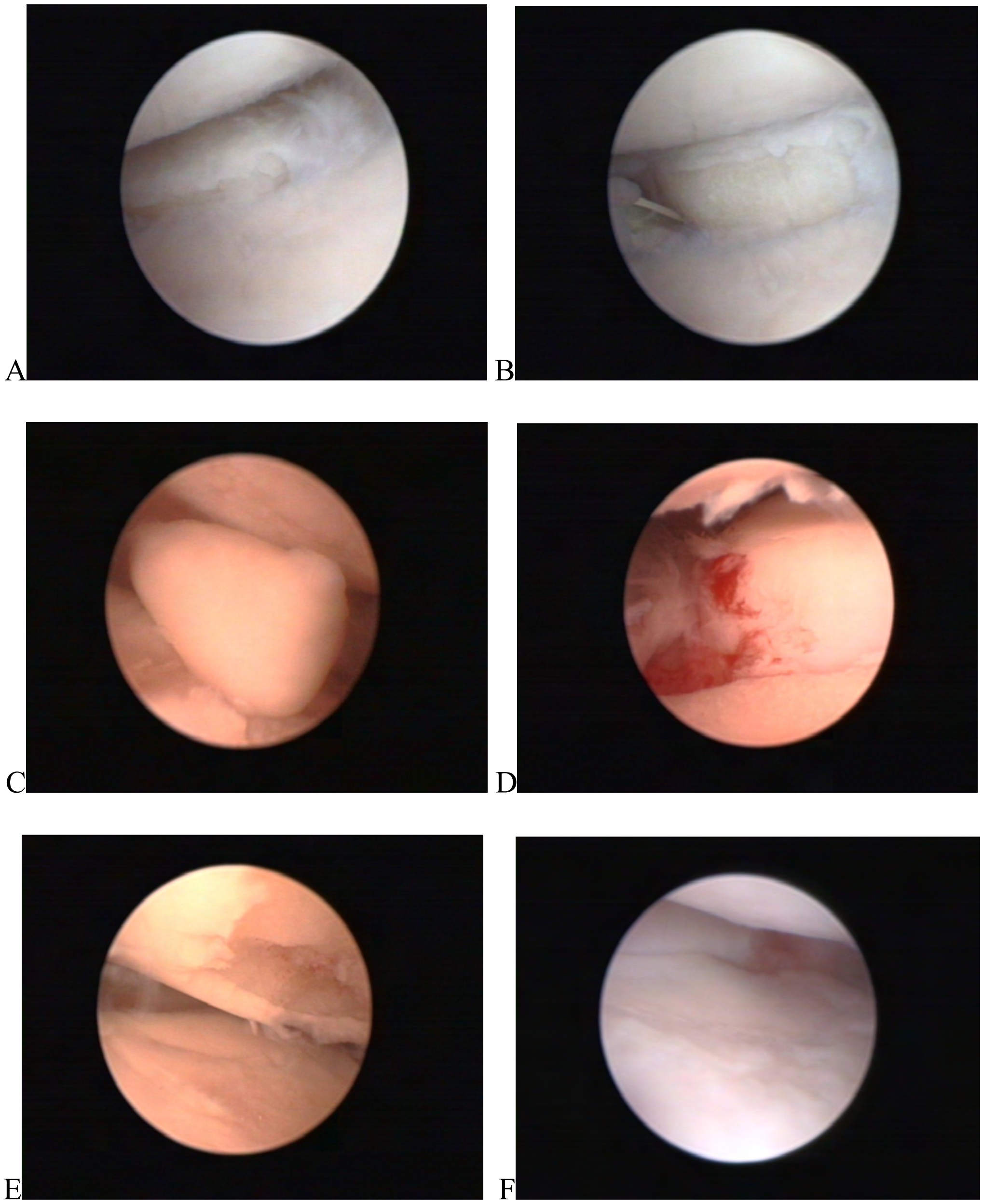

Fig. 35 (A-D) Arthroscopic picture of a 2-year-old Bernese Mountain dog's elbow with fragmented medial coronoid process
(A) Line of fragmentation of medial coronoid process
(B) Elevated fragment of the medial coronoid process showing the typical yellow discoloration of avascular bone
(C) Large osteochondral fragment
(D) Bleeding of the subchondral bone after abrasion arthroplasty
(E, F) Arthroscopic picture of 1-year-old Labrador elbow which has in situ fragment of the medial coronoid process.

3.4 Comparison of radiographic findings and CT findings

A comparison of the calculated accuracy, sensitivity, specificity, positive-predictive value, and negative-predictive value for each technique was performed in Table 6. Both techniques have no difference about accuracy and specificity, but CT has higher sensitivity than radiography.

Table 7: Accuracy, sensitivity, specificity, positive and negative predictive values calculated for each of the techniques to identify FMCP

parameter	CT	Radiography
Accuracy	87%	86%
Sensitivity	86%	57%
Specificity	100%	88%
Positive predictive value	37%	29%
Negative predictive value	100%	97%

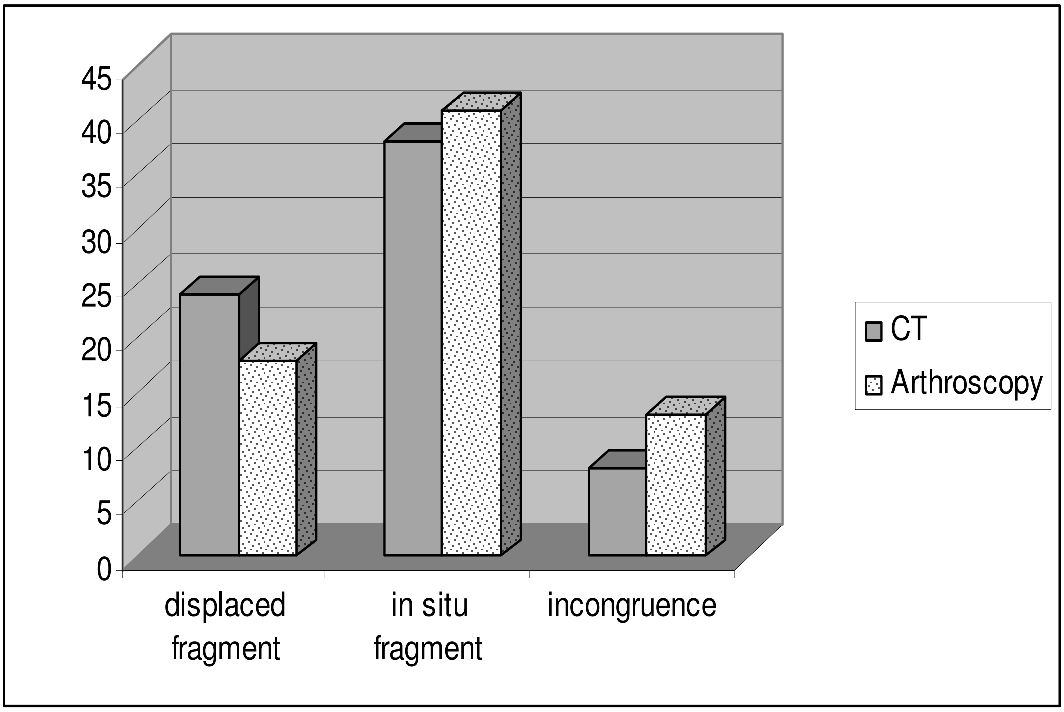

Fig. 36 Box Plot of Numbers of dogs with Arthroscopic- and CT lesions of 92 joints with FMCP